Article

Structure

Cryo-electron tomography reveals the packaging pattern of RuBisCOs in *Synechococcus* β-carboxysome

Graphical abstract

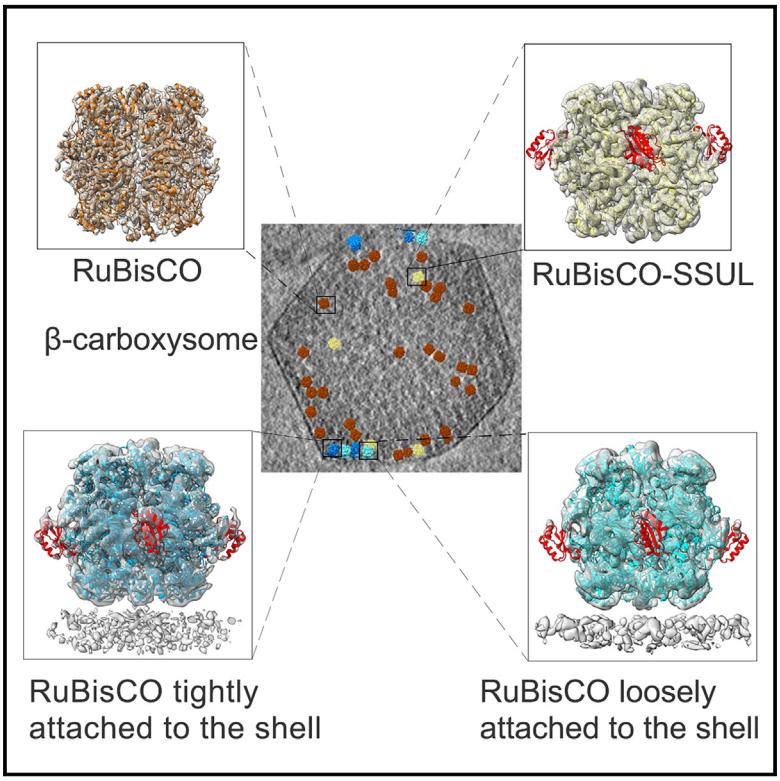

Authors

Wen-Wen Kong, Yun Zhu, Heng-Rui Zhao, ..., Fei Sun, Yong-Liang Jiang, Cong-Zhao Zhou

Correspondence

feisun@ibp.ac.cn (F.S.), jyl@ustc.edu.cn (Y.-L.J.), zcz@ustc.edu.cn (C.-Z.Z.)

In brief

Cyanobacterial carboxysomes are a well-studied bacterial microcompartment that accumulates CO_2 to enhance the carbon fixation efficiency of encapsulated RuBisCOs. Kong et al. elucidated the structures and packaging patterns of internal RuBisCOs in intact β-carboxysomes through cryo-ET analysis, which is a step forward for building the artificial carbon-fixation machinery.

Highlights

- RuBisCOs are densely packed in β-carboxysomes in a lattice-like arrangement
- The adjacent RuBisCOs are usually aligned in three distinct manners
- An ideal model is proposed for the packaging of RuBisCOs in β-carboxysomes

Kong et al., 2024, Structure *32*, 1–11
August 8, 2024
https://doi.org/10.1016/j.str.2024.05.007

CellPress

Structure

CellPress

Article

Cryo-electron tomography reveals the packaging pattern of RuBisCOs in *Synechococcus* β-carboxysome

Wen-Wen Kong,[1,4] Yun Zhu,[2,4] Heng-Rui Zhao,[1] Kang Du,[1] Rui-Qian Zhou,[1] Bo Li,[1] Feng Yang,[1] Pu Hou,[1] Xia-He Huang,[3] Yuxing Chen,[1] Ying-Chun Wang,[3] Fei Sun,[2,*] Yong-Liang Jiang,[1,*] and Cong-Zhao Zhou[1,5,*]

[1]School of Life Sciences, Division of Life Sciences and Medicine, University of Science and Technology of China, Hefei 230026, China
[2]National Key Laboratory of Biomacromolecules, CAS Center for Excellence in Biomacromolecules, Institute of Biophysics, Chinese Academy of Sciences, Beijing 100101, China
[3]Institute of Genetics and Developmental Biology, Chinese Academy of Sciences, Beijing 100101, China
[4]These authors contributed equally
[5]Lead contact
*Correspondence: feisun@ibp.ac.cn (F.S.), jyl@ustc.edu.cn (Y.-L.J.), zcz@ustc.edu.cn (C.-Z.Z.)
https://doi.org/10.1016/j.str.2024.05.007

SUMMARY

Carboxysomes are large self-assembled microcompartments that serve as the central machinery of a CO_2-concentrating mechanism (CCM). Biogenesis of carboxysome requires the fine organization of thousands of individual proteins; however, the packaging pattern of internal RuBisCOs remains largely unknown. Here we purified the intact β-carboxysomes from *Synechococcus elongatus* PCC 7942 and identified the protein components by mass spectrometry. Cryo-electron tomography combined with subtomogram averaging revealed the general organization pattern of internal RuBisCOs, in which the adjacent RuBisCOs are mainly arranged in three distinct manners: head-to-head, head-to-side, and side-by-side. The RuBisCOs in the outermost layer are regularly aligned along the shell, the majority of which directly interact with the shell. Moreover, statistical analysis enabled us to propose an ideal packaging model of RuBisCOs in the β-carboxysome. These results provide new insights into the biogenesis of β-carboxysomes and also advance our understanding of the efficient carbon fixation functionality of carboxysomes.

INTRODUCTION

The photosynthetic organisms, such as plants and algae, can fix CO_2 via the Calvin-Benson-Bassham (CBB) cycle, which annually drives ~120 billion tons of carbon assimilation into sugar.[1] The enzyme ribulose-1,5-bisphosphate carboxylase/oxygenase (RuBisCO), which is the most abundant enzyme on Earth,[2] catalyzes the fixation of CO_2 to ribulose-1,5-bisphosphate (RuBP), producing two molecules of 3-phosphoglycerate (3-PGA). However, RuBisCO is of rather low efficiency in different photosynthetic organisms, owing to its slow catalytic rate and poor capability to discriminate between the two competitive substrates, CO_2 and O_2. Notably, the cyanobacterial RuBisCOs have a much lower affinity toward both CO_2 and O_2, but a higher catalytic rate, compared to those of plant RuBisCOs.[3]

Despite comprising only < 0.2% biomass of photosynthetic organisms, cyanobacteria contribute to > 35% of global biological CO_2 fixation.[4] Over a long evolutionary history, cyanobacteria have evolved a special CO_2-concentrating mechanism (CCM) to accumulate CO_2 molecules at the active sites of RuBisCO, therefore providing a higher CO_2/O_2 ratio for the carbon fixation.[5] The CCM consists of various carbon uptake systems, and the carbon-fixation machinery, termed carboxysome, a well-investigated bacterial microcompartment (BMC).[6–8] The extracellular HCO_3^- is pumped into the cell via the carbon uptake systems and subsequently diffuses into the carboxysome, where it is converted into CO_2 catalyzed by the encapsulated carbonic anhydrase (CA).[9,10] Eventually, the high level CO_2 within the carboxysome maximizes the carboxylation activity of encapsulated RuBisCO, as well as reducing the photorespiration of RuBisCO, therefore enhancing the CO_2 fixation efficiency.[11,12]

The carboxysome is a large self-assembly of about 100–400 nm in diameter,[8] which contains an icosahedral-like proteinaceous shell that encapsulates the cargo enzymes of RuBisCO and CA. Based on the encapsulated RuBisCO, carboxysomes are divided into two types, α- and β-carboxysome.[13] They share a similar overall architecture and functionality but differ in the type of RuBisCO and scaffolding proteins. The α-carboxysomes that contain form IA RuBisCO globally dominate most aquatic habitats,[14] whereas the β-carboxysomes harboring form IB RuBisCO are mainly found in freshwater cyanobacteria.[11] Both α- and β-carboxysomes possess a similar icosahedral shell, which is composed of BMC hexamers and trimers forming the shell facets, in addition to the pentamers that cap the shell vertices.[15–17] The BMC hexamers, which are characterized by a central pore presumably required for the transport of polar

Please cite this article in press as: Kong et al., Cryo-electron tomography reveals the packaging pattern of RuBisCOs in *Synechococcus* β-carboxysome, Structure (2024), https://doi.org/10.1016/j.str.2024.05.007

molecules, constitute the predominant building blocks of the shell.[18–21]

Compared to the α-carboxysome that is encoded by genes mainly in a single *cso* operon,[22] the genes encoding the components of β-carboxysome are distributed in multiple operons and show significant variations among species.[11] The intact β-carboxysome is composed of an icosahedral-like shell encapsulating the inner cargo enzymes,[23] which are crosslinked by two scaffolding proteins: the highly abundant CO_2-concentrating mechanism protein M (CcmM) in addition to the low-abundancy CO_2-concentrating mechanism protein N (CcmN).[23–25] CcmM in *Synechococcus elongatus* PCC 7942 is present in two forms: the full-length CcmM58 and a truncated form CcmM35, possibly resulting from internal ribosome entry sites within the *ccmM* transcript.[26] CcmM58 consists of an N-terminal γ-carbonic anhydrase-like (γCAL) domain followed by three repetitive RuBisCO small subunit-like (SSUL) modules, whereas CcmM35 has only three SSUL modules. The γCAL domain forms a stable heterotrimeric complex with CcmN,[27] which bridges the shell via directly binding to the shell proteins CcmK2, CcmO, and CcmL.[25,27] The repetitive SSUL modules of CcmM58 and CcmM35 specifically bind to RuBisCOs, which are eventually crosslinked to form a liquid-like condensate.[28,29]

The previous cryo-electron tomography (cryo-ET) studies of α-carboxysomes revealed that RuBisCOs are organized in four concentric layers in the marine α-cyanobacterium *Cyanobium* sp. PCC 7001,[30,31] whereas RuBisCOs adopt intertwining spirals in a chemoautotrophic bacterium *Halothiobacillus neapolitanus*.[32] Notably it was found that *H. neapolitanus* RuBisCOs polymerize within α-carboxysome via the small subunits of RuBisCO, which can further pack into a lattice with a 6-fold pseudo-symmetry. Compared to α-carboxysome, the β-carboxysome shows a much higher heterogeneity and dynamics, which involves the ordered organization of thousands of individual proteins. Previous *in vivo* studies indicated that β-carboxysome likely adopts an "inside-out" assembly pattern,[24] in which the CcmM-crosslinked RuBisCO condensates form the core, enabling the recruitment of shell proteins for the formation of intact β-carboxysome.[28,29] However, the internal organization pattern of RuBisCOs in natural β-carboxysome remains largely unknown.

Using cryo-ET and subtomogram averaging (STA), here we determined the structure and internal arrangement of RuBisCOs within the intact β-carboxysome. The results revealed that the *ex vivo* β-carboxysomes are intrinsically heterogeneous, varying greatly in size and shape. We performed the cryo-ET analysis of intact β-carboxysomes and revealed some regular patterns of densely packed RuBisCOs. Together with previous reports,[23,33] we propose an ideal model for the fine packaging of RuBisCOs within the β-carboxysome. These findings advance our understanding on the self-assembly mechanism and functionality of carboxysome.

RESULTS

Purification and biochemical analyses of *Synechococcus* β-carboxysomes

The β-carboxysome of model cyanobacterium *S. elongatus* PCC 7942 (termed *Synechococcus* for short) is encoded by four operons, which have 11 genes in total (Figure 1A). The genes *ccmK2/K3/K4*, *ccmO*, and *ccmP* encode the hexameric or trimeric shell proteins that constitute the shell facets,[34,35] whereas *ccmL* encodes the pentameric shell proteins that fill the shell vertices. The genes *rbcL* and *rbcS* encode the large and small subunits of RuBisCO, respectively; whereas *ccaA* encodes the carbonic anhydrase. In addition, the genes *ccmM* and *ccmN* encode the two scaffolding proteins that crosslink the shell and interior enzymes.[11]

Using the Mg^{2+}/Percoll precipitation method,[36] we pooled all the β-carboxysomes in the cell lysate, which differs from the previously reported method that only separated a subset of β-carboxysomes.[23] The cryo-EM analysis showed that most of purified β-carboxysomes are intact in morphology (Figure 1B). The liquid chromatography mass spectrometry analysis of this β-carboxysome sample also indicated that all protein components are detectable (Table 1). In agreement with the previous proteomic analysis of *Synechococcus*,[23,33] RuBisCO large and small subunits RbcL and RbcS are the most abundant components, followed by the hexameric shell protein CcmK2 and the scaffolding protein CcmM, whereas CcmK3, CcmL, and CcmN are of much lower abundance. Furthermore, the gel electrophoresis analysis also confirmed the individual components, including CcmM58, RbcL, CcmM35, CcaA, CcmO, CcmL/CcmK4/RbcS, and CcmK2 (Figure 1C).

Cryo-electron tomography analysis of intact *Synechococcus* β-carboxysomes

To investigate the packaging pattern of major cargo enzyme RuBisCO within β-carboxysome, the purified β-carboxysome sample was subjected to cryo-ET analysis (Figure 2A). We collected 88 tilt series and reconstructed the tomograms. It was shown that *Synechococcus* β-carboxysomes are rather heterogeneous, differing in shape and size (Figure S1), as also observed in the cells.[38] Therefore, the deformation of β-carboxysomes mainly resulted from the intrinsic heterogeneity in *Synechococcus elongatus* PCC 7942 but not from the squeezing effect in the vitreous ice layer. Beyond the majority that possesses a regular icosahedral-like shape, we also observed several elongated carboxysomes as long as 300–400 nm in the long axis and ~200 nm in the short axis (Figure S1). In fact, the *ex vivo* β-carboxysomes vary greatly in size, ranging from 150 to 400 nm, showing a normal distribution pattern centered at 193 nm (Figure 2B). These results clearly showed the rather high heterogeneity of β-carboxysomes, which differ from the α-carboxysomes of much smaller size.[30,31]

We deconvoluted the tomograms using the software Warp[39] and found that the β-carboxysome shell is generally ~3 nm in thickness (Figure 2C). However, we also observed some scattered ~6 nm-thick patches in the shell (Figure 2C), highlighting the heterogeneity of the shell. As shown previously, the recombinant β-carboxysome shell of *Halothece* sp. PCC 7418 possesses a single-layered structure of 3 nm in thickness,[40] whereas the recombinant BMC shell of *Haliangium ochraceum* has some double-layered protrusions formed by BMC-T pseudohexamers.[41] Accordingly, we propose that the *Synechococcus* β-carboxysome shell is mainly single-layered, with scattered double-layered protrusions, most likely composed of CcmP pseudohexamers[35] and/or CcmK3/K4 dodecamers[42] on the shell.

Please cite this article in press as: Kong et al., Cryo-electron tomography reveals the packaging pattern of RuBisCOs in *Synechococcus* β-carboxysome, Structure (2024), https://doi.org/10.1016/j.str.2024.05.007

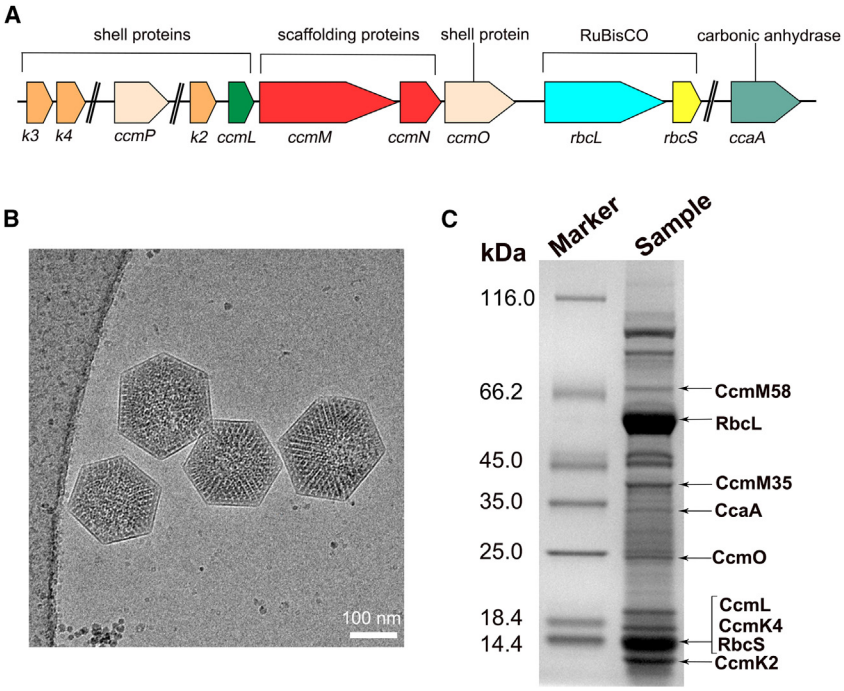

Figure 1. Purification and biochemical characterization of β-carboxysomes from *Synechococcus elongatus* PCC 7942

(A) Organization of the operons encoding the β-carboxysome components. The genes are labeled at the bottom whereas the protein functions are marked on the top.

(B) A representative cryo-EM image of β-carboxysome samples. Scale bar: 100 nm.

(C) SDS-PAGE analysis of the purified β-carboxysomes. Totally nine protein components of β-carboxysome could be identified on the right panel of the gel, with the proteins labeled. The standard protein marker is loaded on the left of the gel, with the molecular weight of each protein band labeled on the left.

The interior of β-carboxysome is full of densely packed RuBisCOs, which form regular radial lattices pointing to the center of carboxysome (Figure 2A), in agreement with the negative-staining electron microscopy results of *Synechococcus* β-carboxysome.[23] We manually counted all RuBisCO particles from 61 intact β-carboxysomes and calculated the density of RuBisCOs in each β-carboxysome. The results showed that the number of RuBisCO is proportionally correlated with the volume of carboxysome (Figure 2D). In a β-carboxysome of 193 nm in diameter or 2.2 × 10^6 nm^3 in volume, in total ~1200 RuBisCOs were observed. The average RuBisCO density in β-carboxysome is generally higher than 650 μM and in some cases up to 1,150 μM (Figure 2D, right panel). In contrast, RuBisCO in *H. neapolitanus* α-carboxysome has a highest concentration up to ~850 μM, and is capable of forming fibers in the internal central region at a concentration exceeding 650 μM.[32] It also indicated that RuBisCOs in β-carboxysome are more densely packed than those in α-carboxysome.

Overall arrangement of RuBisCO within the β-carboxysome

Using the cryo-ET subtomogram averaging, we analyzed the packaging pattern of RuBisCOs within the purified β-carboxysomes. However, the densely packed RuBisCOs posed a significant challenge for accurate alignment of the RuBisCO particles. To overcome this obstacle, we manually picked the free RuBisCO particles outside of the carboxysomes and obtained a 3.9 Å structure of RuBisCO (Figures 3 and S2). Using this RuBisCO structure as a template, we picked all RuBisCO particles using template matching. After several rounds of 3D classifications using different symmetries, we eventually yielded two maps at 4.4 and 5.9 Å resolutions, respectively (Figures 3 and S2). The 3.9 Å structure of RuBisCO could perfectly match the 4.4 Å map, leaving no additional discernible density (Figure 4A). In contrast, fitting the 3.9 Å RuBisCO structure to the 5.9 Å map revealed an extra density around the equator of RuBisCO, corresponding to the binding site of SSUL module of CcmM, which was previously identified by Wang et al.[28] One SSUL module could be roughly fitted into this extra density (Figure 4B), with a local cross-correlation (CC) value of 0.41. Notably, the helix α1 of SSUL perfectly matches the corresponding density, yielding a much higher CC value of 0.65. Vice versa, superposition of our RuBisCO-SSUL model to the previously reported complex structure[28] showed that the SSUL module exactly occupies the same position on RbcL in a similar conformation (Figure S3). It indicated that it is reliable to model the SSUL module to this extra density, despite the low resolution of the extra map. The low-quality map of SSUL modules may be resulted from the high dynamics of SSUL modules binding to RuBisCO, which is influenced by several factors. For instance, only a portion of the four potential SSUL-binding sites on a single RuBisCO molecule may be occupied by SSUL. In addition, the SSUL module may undergo conformational changes to adapt to the variable distance between adjacent RuBisCO molecules.

Template matching and mapping back the positions and orientations of RuBisCO to the original tomograms enabled us to elucidate its overall packaging patterns in the β-carboxysome. The internal RuBisCO is generally arranged in a lattice-like pattern (Figure 2A). It was known that in *Cyanobium* sp. PCC 7001 α-carboxysome, RuBisCOs are aligned in a radial direction with their 4-fold axes roughly pointing to the center of carboxysome.[30] However, statistical analyses showed that RuBisCOs in β-carboxysome showed various orientations, with their 4-fold axes pointing to different directions. It indicated that, despite sharing a lattice-like pattern like α-carboxysome, RuBisCOs in β-carboxysome show a drastic plasticity and divergent arrangements (Video S1). Notably, in the outermost layers of β-carboxysome, the densely packed RuBisCOs are aligned along the shell facets and showed a regular arrangement pattern (Video S1). To better understand the inter-RuBisCO arrangement, we statistically analyzed the distance and intersection

Please cite this article in press as: Kong et al., Cryo-electron tomography reveals the packaging pattern of RuBisCOs in *Synechococcus* β-carboxysome, Structure (2024), https://doi.org/10.1016/j.str.2024.05.007

Table 1. Proteomic results of isolated β-carboxysomes from *Synechococcus*

Gene symbol	Score	Mol. weight [kDa]	coverage	Intensity	iBAQ	Normalized amount
RbcS	99.837	13.333	13.333	5,064,700,000	844,110,000	16,732
RbcL	323.31	52.447	52.447	14,816,000,000	644,160,000	12,769
CcmK2	92.441	10.904	10.904	1,758,700,000	293,120,000	5,810
CcmM	299.55	57.832	57.832	7,645,900,000	238,940,000	4,736
CcmK4	52.549	11.945	11.945	290,230,000	36,279,000	719
CcaA	56.772	30.185	30.185	267,120,000	29,680,000	588
CcmP	53.859	23.2	23.2	39,004,000	3,250,300	64
CcmO	46.296	29.43	29.43	14,088,000	828,680	16
CcmK3	51.023	10.794	10.794	2,331,300	777,090	15
RbcX	16.343	16.982	16.982	4,254,900	709,150	14
CcmL	7.137	11.016	11.016	1,149,100	383,020	7.6
Raf1	21.526	40.159	40.159	4,869,700	270,540	5.4
CcmN	8.7355	16.327	16.327	302,700	50,449	1

angle of the central 4-fold axis in each pair of RuBisCOs. The results revealed three prominent configurations of two adjacent RuBisCOs, which we termed head-to-head, head-to-side, and side-by-side, accounting for ~10%, 17%, and 12% of the total RuBisCO pairs, respectively (Figures 4C and 4D). The head-to-head RuBisCO pairs are respectively located in two neighboring layers, with their 4-fold axes roughly overlapped. By contrast, the adjacent RuBisCOs in the same layer are generally aligned in a head-to-side or side-by-side manner (Figure 4C). Notably, besides these three regular configurations, we also observed some randomly stacked RuBisCO pairs, which have varying tilt angles between the 4-fold axis. Further analysis revealed that the SSUL-bound RuBisCOs are ubiquitously distributed in the β-carboxysome (Figure S4), further confirming that the CcmM harboring repetitive SSUL modules functions as a molecular thread to crosslink the adjacent RuBisCOs.[28] Indeed, we could clearly observe the thread-like densities in the tomograms among RuBisCO particles (Figure S5A), which most likely correspond to the linker region between SSUL modules of CcmM. Statistical analysis demonstrated that the length distribution of the densities is about 2–8 nm, with a median of 3.9 nm (Figures S5A and S5B). To further gain insights into the crosslinking of RuBisCO mediated by SSUL modules, we modeled the mode of SSUL modules binding to two adjacent RuBisCOs (Figure S6). The results showed that the two tandem SSUL modules could effectively link the neighboring RuBisCO particles of varying orientations (Figure S6). Notably, given the 35-residue inter-SSUL linker extends up to a maximum length of 11 nm, the two tandem SSUL modules are limited to crosslink the closest binding sites between two adjacent RuBisCOs. Altogether, our results provided direct evidence that the scaffolding protein CcmM harboring repetitive SSUL modules makes multivalent interactions with RuBisCOs.

The RuBisCOs at the outermost layer of β-carboxysome are regularly aligned

In the outermost layer, the RuBisCOs are generally aligned in a rather dense and regular manner, with their 4-fold axis almost perpendicular to the shell (Figures 5A and 5B). To further investigate the interactions of RuBisCOs in the outermost layer with the shell, we extracted the shell and the outermost layer using the Dynamo[43] surface models for subtomogram analysis (Figure 3). The 3D classification yielded two different classes that account for about 30% and 18% of the total particles in the layer, respectively, which enabled us to construct two maps at 8.0 and 8.4 Å, respectively (Figures 3 and S2). By fitting the atomic coordinates of 3.9 Å RuBisCO structure into the two cryo-EM maps, respectively, we observed an additional density at the equator of RuBisCO that is not a part of RuBisCO itself. The SSUL module could generally match this density (Figures 5C and 5D), indicating that RuBisCOs in the two classes are mostly stabilized by SSUL modules.

The slice views using the software IMOD[37] revealed that RuBisCO in the 8.0 Å map is tightly associated with the shell (Figure 5E), whereas RuBisCO in the 8.4 Å cryo-EM map does not directly interact with the shell (Figure 5F). It suggested that ~30% RuBisCOs in the outermost layer are tightly attached to the shell, probably forming direct interactions with the shell (Figures 5A and 5E). In contrast, about 18% RuBisCOs in the outermost layer are loosely attached to the shell without direct interactions (Figures 5B and 5F). Notably, besides these two major classes, we also observed that some RuBisCOs are completely dissociated from the shell, but remaining linked to the shell via a linear density (Figure S5C), with a median of ~4.6 nm (Figure S5D). This substantial space between RuBisCO and shell is reminiscent of the previous reports that CcmM and CcmM-CcmN directly bridge RuBisCO to the inner surface of the shell.[27,44] We therefore propose that this thin density might accommodate the trimeric γCAL of CcmM or CcmM-CcmN heterocomplex. Noticeably, given a much lower abundance of CcmN compared to CcmM,[23] the RuBisCOs are bridged to the shell mainly by the CcmM trimer but not the CcmM-CcmN heterocomplex.

An ideal model of the orderly packed RuBisCOs in β-carboxysome

The purified β-carboxysomes exhibit an overall heterogeneous morphology of various diameters (Figure S1), thus it is not feasible to obtain the averaged map of β-carboxysome using subtomogram averaging. Instead, we selected three

Please cite this article in press as: Kong et al., Cryo-electron tomography reveals the packaging pattern of RuBisCOs in *Synechococcus* β-carboxysome, Structure (2024), https://doi.org/10.1016/j.str.2024.05.007

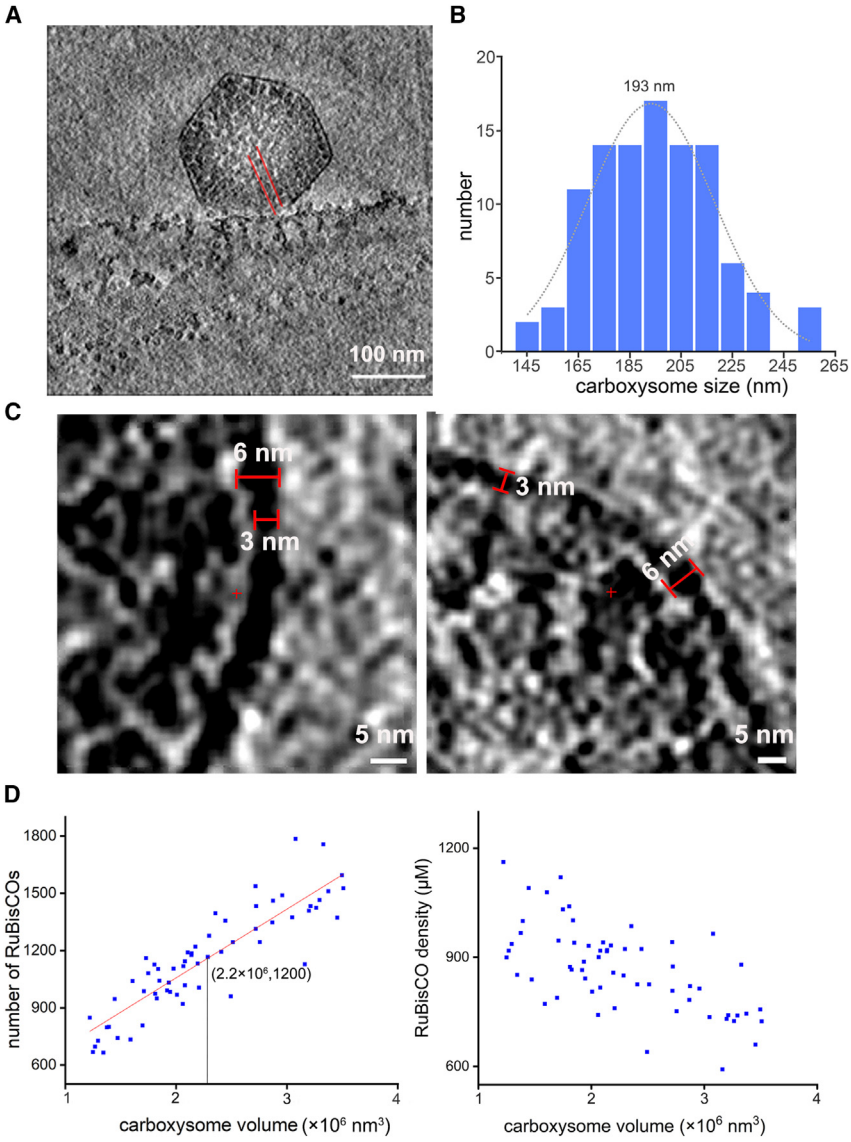

Figure 2. Cryo-ET analysis of β-carboxysome

(A) A slice of the reconstructed tomogram of β-carboxysome. The red lines indicate the radial lattice arrangement of RuBisCO. Scar bar: 100 nm.

(B) Histogram of the normal distributions of the diameters of β-carboxysomes measured from cryo-ET images. The average diameter of 193 nm is labeled.

(C) Selected slices of the carboxysome shell. The representative regions of 3 nm or 6 nm thick are marked with red bars. The red cross indicates the center of the image. All tomograms are deconvolved using Warp and are displayed using IMOD.[37] Scar bar: 5 nm.

(D) Statistics of the total number and the density of RuBisCOs in each carboxysome with different volumes. The carboxysome with a diameter of 193 nm and a volume of 2.2×10^6 nm^3 contains about 1,200 RuBisCOs.

representative β-carboxysomes from the tomograms, with a diameter of approximately 160, 200, and 250 nm, respectively. Afterward, we segmented the β-carboxysomes from the tomograms using EMAN2[45] and reconstructed the cryo-EM maps without applying symmetry. However, these unsymmetrized maps appeared incomplete due to the low signal-to-noise ratio of the tomograms and the missing wedge effect (Figure S7, left panel). Alternatively, we applied I1 symmetric operations against the unsymmetrized maps to generate corresponding icosahedral maps (Figure S7, middle panel). Calculation of the FSC plots between the unsymmetrized and icosahedral maps revealed that all three pairs of maps had rather low resolutions (Figure S7, right panel). It suggested that the β-carboxysomes in our sample do not exhibit a perfect icosahedral shape, but rather an icosahedral-like structure.

Despite the overall heterogeneous morphology of β-carboxysomes, we observed some patches or subtomograms are constituted by regularly aligned RuBisCOs. As shown in Figure 6A, in a sliced single facet in the outermost layer, we can see the regular arrangement of RuBisCOs. Deduced from these regular patches, we built an ideal model of RuBisCOs assembled in the icosahedral-like β-carboxysome. We assumed that the β-carboxysome is an ideal icosahedron, as indicated by the projections at three different symmetric axes (Figure 6B). In this ideal model, the number of RuBisCOs in each facet is generally arranged into an arithmetic progression (Figure 6B). Therefore, we deduced the number of RuBisCO in each facet equals $\sum_{i=1}^{n-3} i$, where n is the average number of RuBisCO on the edge of an icosahedron. Given a total of 12 vertices (each having one RuBisCO) and 30 edges (each having *n*-2 RuBisCOs), the total number (N) of RuBisCOs in the outermost layer should follow the formula $N = 10n^2\text{-}20n\text{+}12$. We selected seven regular carboxysomes with the edge lengths ranging from 101 to 131 nm, and each edge is capable of accommodating 7, 8, or 9 RuBisCOs. According to the formula, the theoretical number of RuBisCOs in the outermost layer is 362, 492, and 642, respectively, which roughly matched the numbers of our counted RuBisCOs (Table 2).

Further analysis of the 45 tomograms of carboxysome showed that the arrangement of RuBisCO in the inner layers of β-carboxysome also somewhat applies the formula. For instance, we selected two carboxysomes of relatively regular shape, in which the internal RuBisCOs are arranged in 9 and 7 layers, respectively. We manually counted the number of RuBisCO molecules that are distinguishable in the outer layers. The actual numbers of RuBisCOs in the outer layers are comparable to the theoretically calculated values (Table S1). In each layer, the RuBisCOs are arranged in an icosahedral-like pattern, similar to those in the outermost layer. The number of RuBisCOs along the edge of

Please cite this article in press as: Kong et al., Cryo-electron tomography reveals the packaging pattern of RuBisCOs in *Synechococcus* β-carboxysome, Structure (2024), https://doi.org/10.1016/j.str.2024.05.007

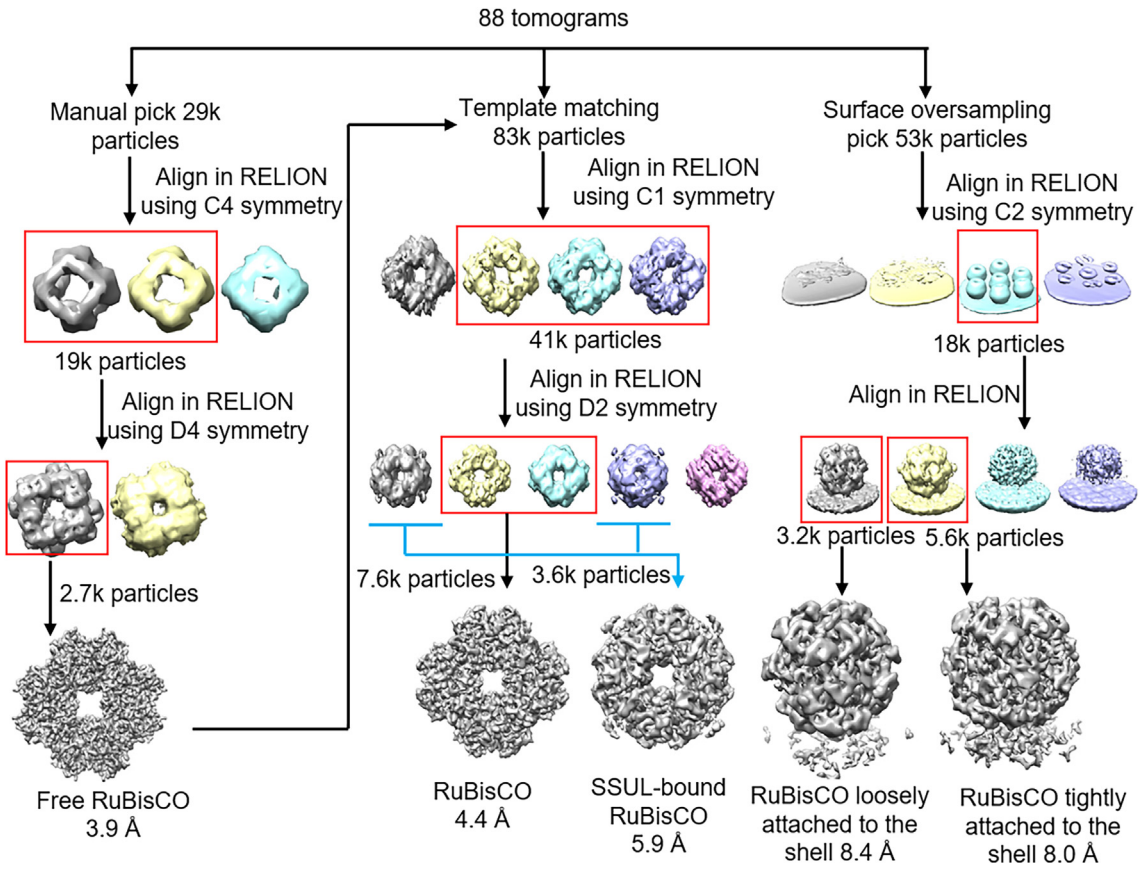

Figure 3. A simplified flowchart for cryo-ET data processing of β-carboxysome

Subtomogram analysis of free RuBisCOs, RuBisCOs within the β-carboxysome and RuBisCOs in the outermost layer of β-carboxysome.

each layer gradually decreased from the outermost to the innermost layer (Figure 6C). The cross-sectional images of β-carboxysome tomograms showed a similar pattern with the projections from the ideal model, which provides evidence for the reliability of the general packaging principle of RuBisCOs. It is worthy to notice that this model is only applied to the icosahedral carboxysomes but not the carboxysomes of irregular shape.

DISCUSSION

The cryo-ET analysis revealed distinct features of the assembly pattern of *Synechococcus* β-carboxysome. First, the β-carboxysomes are rather heterogeneous, varying greatly in shape and size. Besides the icosahedral-like shape, we also observed the elongated β-carboxysomes, which have a maximum diameter of 400 nm. Previous studies have shown that the elongated carboxysomes were commonly observed at the constriction site of the midcell.[24] Moreover, the shell generally has a single layer with a thickness of ~3 nm, in addition to some scattered double layers of ~6 nm in thickness, which may correspond to the shell protein CcmP,[35] CcmK3/K4,[42] or the scaffold proteins attaching to the interior of the shell.[27,44] Second, we observed the direct interactions between RuBisCOs in the outermost layer and the carboxysome shell (Figures 5A and 5C). Third, the RuBisCOs in the outer layers of β-carboxysome are generally arranged in a regular manner, which is mediated by the SSUL modules of CcmM. Indeed, the cryo-ET analysis showed that the SSUL modules run throughout the interior of β-carboxysome, which effectively crosslink the neighboring RuBisCOs (Figures 4B and S6). The tightly packed RuBisCOs in the outer layers are relatively stable and usually remain accumulated together even though the carboxysome shell is broken (Figure S1). These tightly packed RuBisCOs could prevent the diffusion of the reactants, which possibly allows RuBisCO-derived protons to drive the conversion of HCO_3^- to CO_2 via colocalized CA, enhancing both condensate CO_2 and RuBisCO rate.[46] By contrast, loosely packed RuBisCOs are susceptible to be released from the carboxysome and further dissociate into free RuBisCOs once the shell is broken (Figure S1).

Generally, the packaging pattern of RuBisCOs in β-carboxysome is much more complicated and shows a drastic plasticity, which differs from the radial or spiral string pattern of RuBisCO in α-carboxysomes.[30,32] RuBisCOs in α-carboxysome form fiber arrangement mediated by direct interactions of the small subunits CbbS.[30] Despite possessing a much higher RuBisCO density (Figure 2D), the RuBisCOs in β-carboxysome did not display fiber arrangements. Sequence analysis showed that these interacting residues, including Asn23, Glu25, Glu77, Arg80, and Ser81 are not conserved in either α- or β-carboxysomes (Figure S8). These findings suggest that RuBisCO molecules, either

Please cite this article in press as: Kong et al., Cryo-electron tomography reveals the packaging pattern of RuBisCOs in *Synechococcus* β-carboxysome, Structure (2024), https://doi.org/10.1016/j.str.2024.05.007

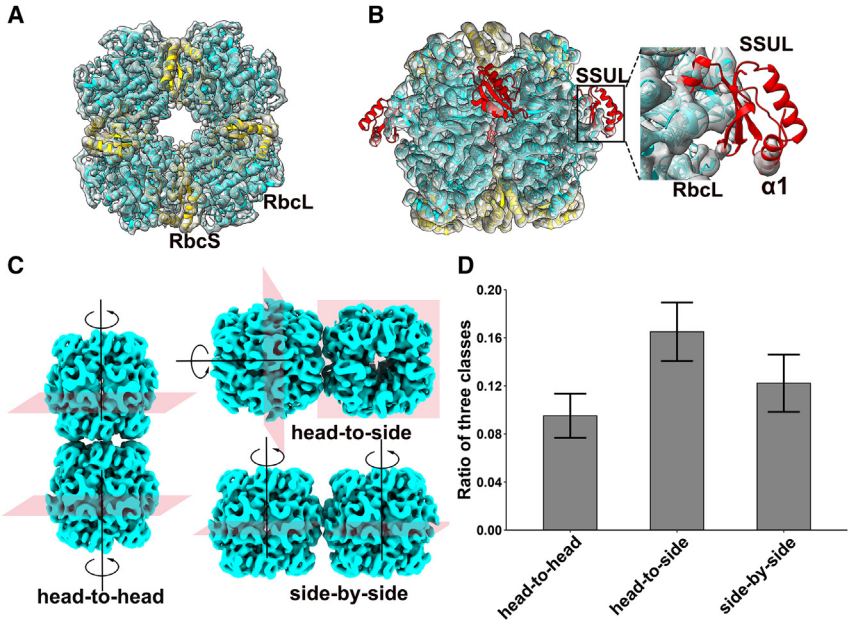

Figure 4. Structures and arrangement of RuBisCOs in the β-carboxysome

(A) Cryo-ET structure of RuBisCO at 4.4 Å resolution. The map is shown in gray surface, whereas the RuBisCO structure is shown in cartoon, with the large and small subunits of RuBisCO colored cyan and yellow, respectively.

(B) Cryo-ET structure of RuBisCO-SSUL at 5.9 Å resolution. The map is shown in gray surface with the structure of RuBisCO-SSUL fitted in the map. The structure of RuBisCO-SSUL is shown in cartoon, with RbcL, RbcS, and SSUL colored cyan, yellow, and red, respectively. The inset represents a zoom-in view of the density corresponding to SSUL. Contour level: 0.0036.

(C) The three prominent patterns of adjacent RuBisCOs are shown. The RuBisCO is shown as cyan surface with its 4-fold axis indicated by a black line. The equator of each RuBisCO is indicated by a pink plane.

(D) Distribution of three prominent patterns of adjacent RuBisCOs from ~26,700 particles. The standard deviation was calculated based on the distribution of the three patterns within these 73 tilt series.

in α- or β-carboxysomes, exhibit diverse packaging patterns. Instead, the adjacent RuBisCO pairs, which are mainly cross-linked by the scaffolding proteins CcmM, but not via direct interactions, show various stacking patterns. In addition, the notable difference between the two types of carboxysomes lies in the distinct crosslinkers that mediate the condensation of

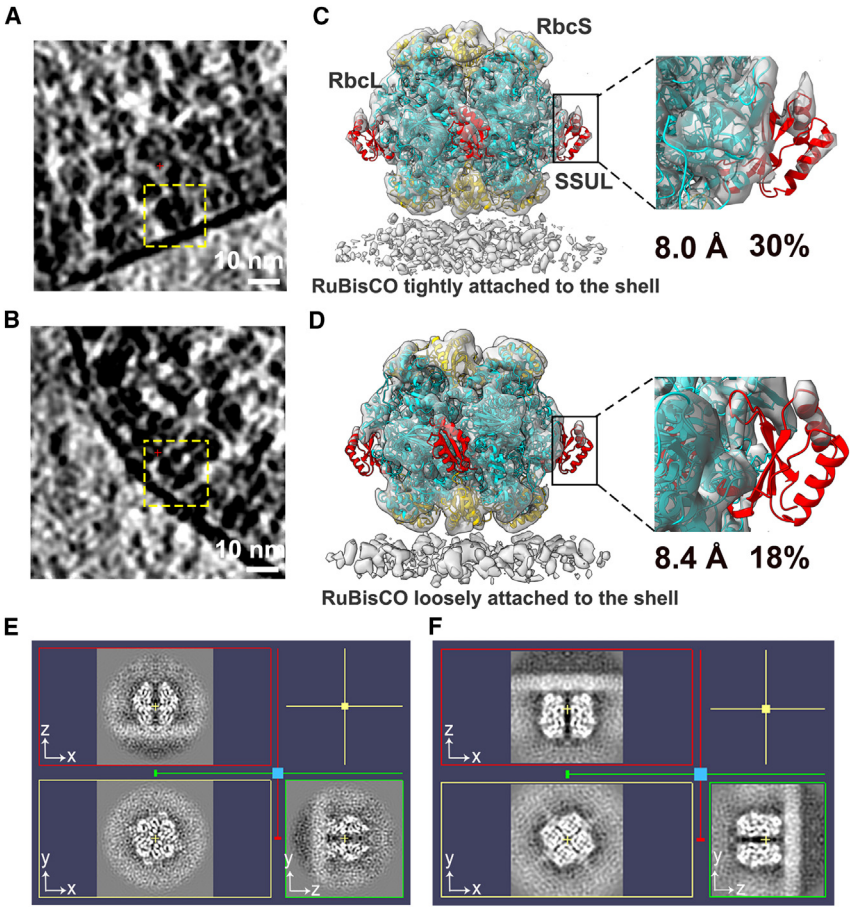

Figure 5. Structures and arrangements of RuBisCOs in the outermost layer of β-carboxysome

(A and B) Selected slices in the outermost layer showing RuBisCOs that are (A) tightly or (B) loosely attached to the shell. The red cross indicates the center of the image. Dotted boxes indicate the tightly or loosely attached RuBisCOs in the outermost layer. Scar bar: 10 nm.

(C and D) Cryo-ET structures of the (C) tightly or (D) loosely attached RuBisCOs at 8.0 Å (contour level: 0.0099) and 8.4 Å (contour level: 0.0083), respectively. The maps are shown in surface with an inset showing the density corresponding to the SSUL module. The structure of RuBisCO-SSUL is fitted into the map, with RbcL, RbcS, and SSUL colored cyan, yellow and red, respectively.

(E and F) Orthogonal slices of the cryo-EM maps using IMOD showing RuBisCOs that are (E) tightly or (F) loosely attached to the shell. The black and white contour levels are set to 40 and 162, respectively in (E), and 54 and 175, respectively in (F).

Please cite this article in press as: Kong et al., Cryo-electron tomography reveals the packaging pattern of RuBisCOs in *Synechococcus* β-carboxysome, Structure (2024), https://doi.org/10.1016/j.str.2024.05.007

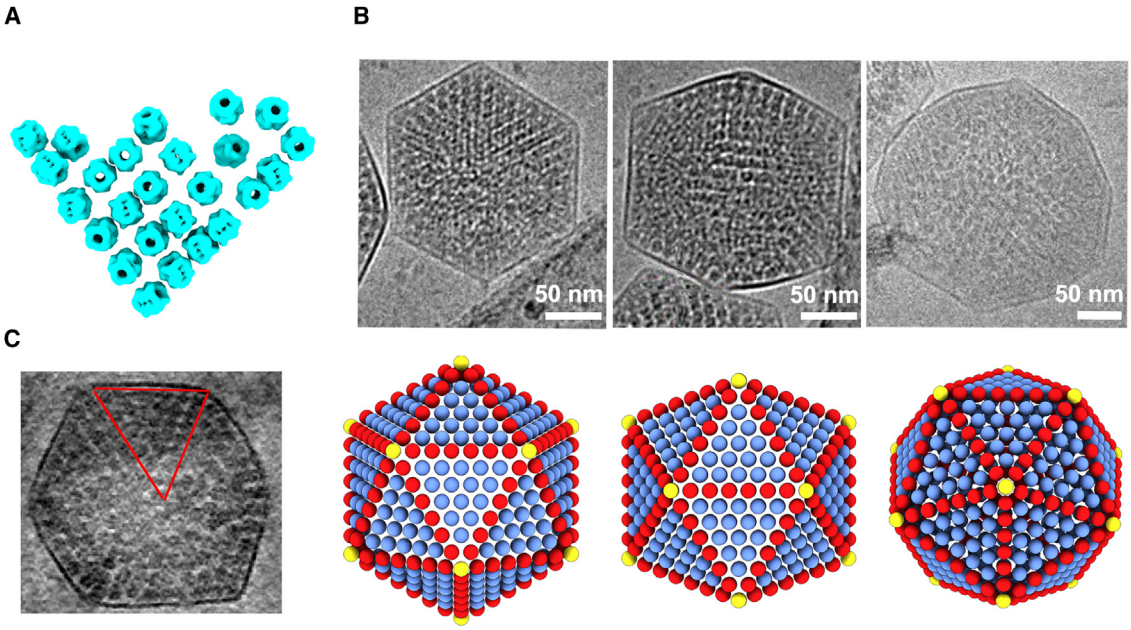

Figure 6. An ideal model of RuBisCOs assembled in the β-carboxysome

(A) The arrangement of RuBisCOs in a single facet in the outermost layer of β-carboxysome.

(B) Cryo-EM images of β-carboxysome observed from the 3-, 2- or 5-fold axis. The corresponding ideal model of RuBisCOs aligned in the outermost layer of carboxysome is shown at the bottom. The RuBisCOs at the facets, edges, and vertices are shown as blue, red, and yellow balls, respectively.

(C) Hexagonal section of the carboxysome. A single facet of the carboxysome is highlighted with a red triangle.

RuBisCOs. Compared to an α-helix of CsoS2 binding to RuBisCO in α-carboxysome,[47] the SSUL modules possess a much higher affinity toward RuBisCO in β-carboxysome.[29] Due to the densely packed pattern crosslinked by SSUL modules, the RuBisCOs encapsulated within the β-carboxysome should not be diffusible, consistent with the previous fluorescence recovery studies.[48]

In summary, we performed the cryo-ET analysis of β-carboxysome, which shed light on the packaging pattern of RuBisCOs in β-carboxysomes. The results provide insights into the self-assembly of β-carboxysome, especially the ordered arrangement of internal RuBisCOs. Given the high heterogeneity of β-carboxysomes, more effective and challenging techniques, such as the high-resolution cellular cryo-ET, are needed to elucidate the fine assembly pattern of all protein components in β-carboxysome.

STAR★METHODS

Detailed methods are provided in the online version of this paper and include the following:

- KEY RESOURCES TABLE
- RESOURCE AVAILABILITY
  - Lead contact
  - Materials availability
  - Data and code availability
- EXPERIMENTAL MODEL AND STUDY PARTICIPANT DETAILS
- METHOD DETAILS
  - Growth of cyanobacteria
  - Purification of β-carboxysomes
  - SDS-PAGE analysis
  - Liquid chromatography mass spectrometry analysis
  - Cryo-ET sample preparation and data collection
  - Tilt series acquisition
  - Image processing

Table 2. The statistics of the number of RuBisCOs at the outermost layer of β-carboxysomes with different sizes

Edge length of carboxysome *L* (nm)	The number of RuBisCOs on icosahedral edges n = ⌊(L-11)/13.2 + 0.5⌋	The theoretical number of RuBisCOs at the outermost layer $10n^2$-20n+12	Manually counted number of RuBisCOs at the outermost layer
101	7	362	367
101	7	362	319
116	8	492	396
111	8	492	375
131	9	642	512
125	9	642	545
127	9	642	529

- Calculation of the volume and RuBisCO density of β-carboxysome
- Statistical analysis of RuBisCO arrangements in β-carboxysome
- The ideal modeling of RuBisCO arrangements in β-carboxysome

- QUANTIFICATION AND STATISTICAL ANALYSIS

SUPPLEMENTAL INFORMATION

Supplemental information can be found online at https://doi.org/10.1016/j.str.2024.05.007.

ACKNOWLEDGMENTS

All cryo-EM datasets were collected at Center for Biological Imaging, Institute of Biophysics, Chinese Academy of Sciences. We are grateful to Xiaojun Huang and Linhua Tai for help with cryo-EM data collection. We thank Gao Wu from the Mass Spectrometry Platform of University of Science and Technology of China. This work was supported by grants from the National Natural Science Foundation of China (http://www.nsfc.gov.cn; 32241025 and 32171198), Strategic Priority Research Program of the Chinese Academy of Sciences (XDB37020301), USTC Research Funds of the Double First-Class Initiative (YD9100002023) and the Key Research and Development Projects of Anhui Province (http://kjt.ah.gov.cn; 2022l07020034 and 202104i07020004). Y.-L.J. thanks the Youth Innovation Promotion Association of Chinese Academy of Sciences for their support (membership no. 2020452).

AUTHOR CONTRIBUTIONS

C.-Z.Z., Y.-L.J., F.S., and Y.C. conceived, designed and supervised this project. W.-W.K., R.-Q.Z., and B.L. performed *Synechococcus elongatus* PCC 7942 growth, β-carboxysome purification, and biochemical assays. X.-H.H. and Y.-C.W. performed liquid chromatography mass spectrometry. W.-W.K. and Y.-L.J. performed cryo-EM sample preparation and data collection. W.-W.K., Y.Z., Y.-L.J., H.-R.Z., K.D., F.Y., and P.H. conducted cryo-ET data processing, structure determination and model building. W.-W.K., Y.-L.J., C.-Z.Z., and Y.Z. wrote and revised the manuscript with input from all authors. All of the authors discussed the data and read the manuscript.

DECLARATION OF INTERESTS

The authors declare no competing interests.

Received: February 1, 2024
Revised: April 1, 2024
Accepted: May 7, 2024
Published: May 31, 2024

REFERENCES

1. Prywes, N., Phillips, N.R., Tuck, O.T., Valentin-Alvarado, L.E., and Savage, D.F. (2023). Rubisco function, evolution, and engineering. Annu. Rev. Biochem. *92*, 385–410. https://doi.org/10.1146/annurev-biochem-040320-101244.
2. Bar-On, Y.M., and Milo, R. (2019). The global mass and average rate of Rubisco. Proc. Natl. Acad. Sci. USA *116*, 4738–4743. https://doi.org/10.1073/pnas.1816654116.
3. Price, G.D., Badger, M.R., Woodger, F.J., and Long, B.M. (2008). Advances in understanding the cyanobacterial CO_2-concentrating-mechanism (CCM): functional components, Ci transporters, diversity, genetic regulation and prospects for engineering into plants. J. Exp. Bot. *59*, 1441–1461. https://doi.org/10.1093/jxb/erm112.
4. Seelke, R. (2007). The Prokaryotes: A Handbook on the Biology of Bacteria, *45* (Choice: Current Reviews for Academic Libraries), p. 68.
5. Kupriyanova, E.V., Sinetova, M.A., Cho, S.M., Park, Y.I., Los, D.A., and Pronina, N.A. (2013). CO_2-concentrating mechanism in cyanobacterial photosynthesis: organization, physiological role, and evolutionary origin. Photosynth. Res. *117*, 133–146. https://doi.org/10.1007/s11120-013-9860-z.
6. Cai, F., Sutter, M., Bernstein, S.L., Kinney, J.N., and Kerfeld, C.A. (2015). Engineering bacterial microcompartment shells: chimeric shell proteins and chimeric carboxysome shells. ACS Synth. Biol. *4*, 444–453. https://doi.org/10.1021/sb500226j.
7. Rottet, S., Förster, B., Hee, W.Y., Rourke, L.M., Price, G.D., and Long, B.M. (2021). Engineered accumulation of bicarbonate in plant chloroplasts: known knowns and known unknowns. Front. Plant Sci. *12*, 727118. https://doi.org/10.3389/fpls.2021.727118.
8. Liu, L.N. (2022). Advances in the bacterial organelles for CO_2 fixation. Trends Microbiol. *30*, 567–580. https://doi.org/10.1016/j.tim.2021.10.004.
9. Blikstad, C., Dugan, E.J., Laughlin, T.G., Turnšek, J.B., Liu, M.D., Shoemaker, S.R., Vogiatzi, N., Remis, J.P., and Savage, D.F. (2023). Identification of a carbonic anhydrase-Rubisco complex within the alpha-carboxysome. Proc. Natl. Acad. Sci. USA *120*, e2308600120. https://doi.org/10.1073/pnas.2308600120.
10. Pulsford, S.B., Nguyen, N.D., and Long, B.M. (2023). The ties that bind: disordered linkers underpin carboxysome construction. Proc. Natl. Acad. Sci. USA *120*, e2316828120. https://doi.org/10.1073/pnas.2316828120.
11. Rae, B.D., Long, B.M., Badger, M.R., and Price, G.D. (2013). Functions, compositions, and evolution of the two types of carboxysomes: polyhedral microcompartments that facilitate CO_2 fixation in cyanobacteria and some proteobacteria. Microbiol. Mol. Biol. Rev. *77*, 357–379. https://doi.org/10.1128/Mmbr.00061-12.
12. Badger, M.R., and Price, G.D. (2003). CO_2 concentrating mechanisms in cyanobacteria: molecular components, their diversity and evolution. J. Exp. Bot. *54*, 609–622. https://doi.org/10.1093/jxb/erg076.
13. Badger, M.R., Hanson, D., and Price, G.D. (2002). Evolution and diversity of CO_2 concentrating mechanisms in cyanobacteria. Funct. Plant Biol. *29*, 161–173. https://doi.org/10.1071/Pp01213.
14. Cabello-Yeves, P.J., Scanlan, D.J., Callieri, C., Picazo, A., Schallenberg, L., Huber, P., Roda-Garcia, J.J., Bartosiewicz, M., Belykh, O.I., Tikhonova, I.V., et al. (2022). Alpha-cyanobacteria possessing form IA RuBisCO globally dominate aquatic habitats. ISME J. *16*, 2421–2432. https://doi.org/10.1038/s41396-022-01282-z.
15. Klein, M.G., Zwart, P., Bagby, S.C., Cai, F., Chisholm, S.W., Heinhorst, S., Cannon, G.C., and Kerfeld, C.A. (2009). Identification and structural analysis of a novel carboxysome shell protein with implications for metabolite transport. J. Mol. Biol. *392*, 319–333. https://doi.org/10.1016/j.jmb.2009.03.056.
16. Tanaka, S., Kerfeld, C.A., Sawaya, M.R., Cai, F., Heinhorst, S., Cannon, G.C., and Yeates, T.O. (2008). Atomic-level models of the bacterial carboxysome shell. Science *319*, 1083–1086. https://doi.org/10.1126/science.1151458.
17. Kerfeld, C.A., Sawaya, M.R., Tanaka, S., Nguyen, C.V., Phillips, M., Beeby, M., and Yeates, T.O. (2005). Protein structures forming the shell of primitive bacterial organelles. Science *309*, 936–938. https://doi.org/10.1126/science.1113397.
18. Dou, Z., Heinhorst, S., Williams, E.B., Murin, C.D., Shively, J.M., and Cannon, G.C. (2008). CO_2 fixation kinetics of *Halothiobacillus neapolitanus* mutant carboxysomes lacking carbonic anhydrase suggest the shell acts as a diffusional barrier for CO_2. J. Biol. Chem. *283*, 10377–10384. https://doi.org/10.1074/jbc.M709285200.
19. Faulkner, M., Szabó, I., Weetman, S.L., Sicard, F., Huber, R.G., Bond, P.J., Rosta, E., and Liu, L.N. (2020). Molecular simulations unravel the molecular principles that mediate selective permeability of carboxysome shell protein. Sci. Rep. *10*, 17501. https://doi.org/10.1038/s41598-020-74536-5.
20. Sarkar, D., Maffeo, C., Sutter, M., Aksimentiev, A., Kerfeld, C., and Vermaas, J. (2024). Atomic view of photosynthetic metabolite permeability pathways and confinement in cyanobacterial carboxysomes. https://doi.org/10.26434/chemrxiv-2024-kbcdf.
21. Trettel, D.S., Pacheco, S.L., Laskie, A.K., and Gonzalez-Esquer, C.R. (2024). Modeling bacterial microcompartment architectures for enhanced

cyanobacterial carbon fixation. Front. Plant Sci. *15*, 1346759. https://doi.org/10.3389/fpls.2024.1346759.

22. Chen, T., Fang, Y., Jiang, Q., Dykes, G.F., Lin, Y., Price, G.D., Long, B.M., and Liu, L.N. (2022). Incorporation of functional Rubisco activases into engineered carboxysomes to enhance carbon fixation. ACS Synth. Biol. *11*, 154–161. https://doi.org/10.1021/acssynbio.1c00311.
23. Faulkner, M., Rodriguez-Ramos, J., Dykes, G.F., Owen, S.V., Casella, S., Simpson, D.M., Beynon, R.J., and Liu, L.N. (2017). Direct characterization of the native structure and mechanics of cyanobacterial carboxysomes. Nanoscale *9*, 10662–10673. https://doi.org/10.1039/c7nr02524f.
24. Cameron, J.C., Wilson, S.C., Bernstein, S.L., and Kerfeld, C.A. (2013). Biogenesis of a bacterial organelle: The carboxysome assembly pathway. Cell *155*, 1131–1140. https://doi.org/10.1016/j.cell.2013.10.044.
25. Kinney, J.N., Salmeen, A., Cai, F., and Kerfeld, C.A. (2012). Elucidating essential role of conserved carboxysomal protein CcmN reveals common feature of bacterial microcompartment assembly. J. Biol. Chem. *287*, 17729–17736. https://doi.org/10.1074/jbc.M112.355305.
26. Ludwig, M., Sültemeyer, D., and Price, G.D. (2008). Isolation of ccmKLMN genes from the marine cyanobacterium, *Synechococcus* sp. PCC7002 (cyanophyceae), and evidence that ccmm is essential for carboxysome assembly. J. Phycol. *36*, 1109–1119. https://doi.org/10.1046/j.1529-8817.2000.00028.x.
27. Sun, H., Cui, N., Han, S.J., Chen, Z.P., Xia, L.Y., Chen, Y., Jiang, Y.L., and Zhou, C.Z. (2021). Complex structure reveals CcmM and CcmN form a heterotrimeric adaptor in beta-carboxysome. Protein Sci. *30*, 1566–1576. https://doi.org/10.1002/pro.4090.
28. Wang, H., Yan, X., Aigner, H., Bracher, A., Nguyen, N.D., Hee, W.Y., Long, B.M., Price, G.D., Hartl, F.U., and Hayer-Hartl, M. (2019). Rubisco condensate formation by CcmM in beta-carboxysome biogenesis. Nature *566*, 131–135. https://doi.org/10.1038/s41586-019-0880-5.
29. Zang, K., Wang, H., Hartl, F.U., and Hayer-Hartl, M. (2021). Scaffolding protein CcmM directs multiprotein phase separation in beta-carboxysome biogenesis. Nat. Struct. Mol. Biol. *28*, 909–922. https://doi.org/10.1038/s41594-021-00676-5.
30. Ni, T., Sun, Y., Burn, W., Al-Hazeem, M.M.J., Zhu, Y., Yu, X., Liu, L.N., and Zhang, P. (2022). Structure and assembly of cargo Rubisco in two native alpha-carboxysomes. Nat. Commun. *13*, 4299. https://doi.org/10.1038/s41467-022-32004-w.
31. Evans, S.L., Al-Hazeem, M.M.J., Mann, D., Smetacek, N., Beavil, A.J., Sun, Y., Chen, T., Dykes, G.F., Liu, L.N., and Bergeron, J.R.C. (2023). Single-particle cryo-EM analysis of the shell architecture and internal organization of an intact alpha-carboxysome. Structure *31*, 677–688.e4. https://doi.org/10.1016/j.str.2023.03.008.
32. Metskas, L.A., Ortega, D., Oltrogge, L.M., Blikstad, C., Lovejoy, D.R., Laughlin, T.G., Savage, D.F., and Jensen, G.J. (2022). Rubisco forms a lattice inside alpha-carboxysomes. Nat. Commun. *13*, 4863. https://doi.org/10.1038/s41467-022-32584-7.
33. Sun, Y., Wollman, A.J.M., Huang, F., Leake, M.C., and Liu, L.N. (2019). Single-organelle quantification reveals stoichiometric and structural variability of carboxysomes dependent on the environment. Plant Cell *31*, 1648–1664. https://doi.org/10.1105/tpc.18.00787.
34. Rae, B.D., Long, B.M., Badger, M.R., and Price, G.D. (2012). Structural determinants of the outer shell of beta-carboxysomes in *Synechococcus elongatus* PCC 7942: roles for CcmK2, K3-K4, CcmO, and CcmL. PLoS One *7*, e43871. https://doi.org/10.1371/journal.pone.0043871.
35. Cai, F., Sutter, M., Cameron, J.C., Stanley, D.N., Kinney, J.N., and Kerfeld, C.A. (2013). The structure of CcmP, a tandem bacterial microcompartment domain protein from the beta-carboxysome, forms a subcompartment within a microcompartment. J. Biol. Chem. *288*, 16055–16063. https://doi.org/10.1074/jbc.M113.456897.
36. Price, G.D., Coleman, J.R., and Badger, M.R. (1992). Association of carbonic anhydrase activity with carboxysomes isolated from the cyanobacterium *Synechococcus* PCC7942. Plant Physiol. *100*, 784–793. https://doi.org/10.1104/pp.100.2.784.
37. Kremer, J.R., Mastronarde, D.N., and McIntosh, J.R. (1996). Computer visualization of three-dimensional image data using IMOD. J. Struct. Biol. *116*, 71–76. https://doi.org/10.1006/jsbi.1996.0013.
38. Kaneko, Y., Danev, R., Nagayama, K., and Nakamoto, H. (2006). Intact carboxysomes in a cyanobacterial cell visualized by hilbert differential contrast transmission electron microscopy. J. Bacteriol. *188*, 805–808. https://doi.org/10.1128/JB.188.2.805-808.2006.
39. Tegunov, D., and Cramer, P. (2019). Real-time cryo-electron microscopy data preprocessing with Warp. Nat. Methods *16*, 1146–1152. https://doi.org/10.1038/s41592-019-0580-y.
40. Sutter, M., Laughlin, T.G., Sloan, N.B., Serwas, D., Davies, K.M., and Kerfeld, C.A. (2019). Structure of a synthetic beta-carboxysome shell. Plant Physiol. *181*, 1050–1058. https://doi.org/10.1104/pp.19.00885.
41. Sutter, M., Greber, B., Aussignargues, C., and Kerfeld, C.A. (2017). Assembly principles and structure of a 6.5-MDa bacterial microcompartment shell. Science *356*, 1293–1297. https://doi.org/10.1126/science.aan3289.
42. Sommer, M., Sutter, M., Gupta, S., Kirst, H., Turmo, A., Lechno-Yossef, S., Burton, R.L., Saechao, C., Sloan, N.B., Cheng, X., et al. (2019). Heterohexamers formed by CcmK3 and CcmK4 increase the complexity of beta carboxysome shells. Plant Physiol. *179*, 156–167. https://doi.org/10.1104/pp.18.01190.
43. Castano-Diez, D., Kudryashev, M., Arheit, M., and Stahlberg, H. (2012). Dynamo: a flexible, user-friendly development tool for subtomogram averaging of cryo-EM data in high-performance computing environments. J. Struct. Biol. *178*, 139–151. https://doi.org/10.1016/j.jsb.2011.12.017.
44. Cai, F., Bernstein, S.L., Wilson, S.C., and Kerfeld, C.A. (2016). Production and characterization of synthetic carboxysome shells with incorporated luminal proteins. Plant Physiol. *170*, 1868–1877. https://doi.org/10.1104/pp.15.01822.
45. Chen, M., Dai, W., Sun, S.Y., Jonasch, D., He, C.Y., Schmid, M.F., Chiu, W., and Ludtke, S.J. (2017). Convolutional neural networks for automated annotation of cellular cryo-electron tomograms. Nat. Methods *14*, 983–985. https://doi.org/10.1038/nmeth.4405.
46. Long, B.M., Förster, B., Pulsford, S.B., Price, G.D., and Badger, M.R. (2021). Rubisco proton production can drive the elevation of CO_2 within condensates and carboxysomes. Proc. Natl. Acad. Sci. USA *118*, e2014406118. https://doi.org/10.1073/pnas.2014406118.
47. Oltrogge, L.M., Chaijarasphong, T., Chen, A.W., Bolin, E.R., Marqusee, S., and Savage, D.F. (2020). Multivalent interactions between CsoS2 and Rubisco mediate alpha-carboxysome formation. Nat. Struct. Mol. Biol. *27*, 281–287. https://doi.org/10.1038/s41594-020-0387-7.
48. Chen, A.H., Robinson-Mosher, A., Savage, D.F., Silver, P.A., and Polka, J.K. (2013). The bacterial carbon-fixing organelle is formed by shell envelopment of preassembled cargo. PLoS One *8*, e76127. https://doi.org/10.1371/journal.pone.0076127.
49. Bharat, T.A.M., and Scheres, S.H.W. (2016). Resolving macromolecular structures from electron cryo-tomography data using subtomogram averaging in RELION. Nat. Protoc. *11*, 2054–2065. https://doi.org/10.1038/nprot.2016.124.
50. Meng, E.C., Goddard, T.D., Pettersen, E.F., Couch, G.S., Pearson, Z.J., Morris, J.H., and Ferrin, T.E. (2023). UCSF ChimeraX: Tools for structure building and analysis. Protein Sci. *32*, e4792. https://doi.org/10.1002/pro.4792.
51. Adams, P.D., Afonine, P.V., Bunkóczi, G., Chen, V.B., Davis, I.W., Echols, N., Headd, J.J., Hung, L.W., Kapral, G.J., Grosse-Kunstleve, R.W., et al. (2010). PHENIX: a comprehensive Python-based system for macromolecular structure solution. Acta Crystallogr. D *66*, 213–221. https://doi.org/10.1107/S0907444909052925.
52. Emsley, P., and Cowtan, K. (2004). Coot: model-building tools for molecular graphics. Acta Crystallogr. D *60*, 2126–2132. https://doi.org/10.1107/S0907444904019158.

53. Ritchie, R.J. (2006). Consistent sets of spectrophotometric chlorophyll equations for acetone, methanol and ethanol solvents. Photosynth. Res. *89*, 27–41. https://doi.org/10.1007/s11120-006-9065-9.

54. Wisniewski, J.R., Zougman, A., Nagaraj, N., and Mann, M. (2009). Universal sample preparation method for proteome analysis. Nat. Methods *6*, 359–362. https://doi.org/10.1038/nmeth.1322.

55. Rappsilber, J., Mann, M., and Ishihama, Y. (2007). Protocol for micro-purification, enrichment, pre-fractionation and storage of peptides for proteomics using StageTips. Nat. Protoc. *2*, 1896–1906. https://doi.org/10.1038/nprot.2007.261.

56. Mastronarde, D.N. (2005). Automated electron microscope tomography using robust prediction of specimen movements. J. Struct. Biol. *152*, 36–51. https://doi.org/10.1016/j.jsb.2005.07.007.

57. Wu, C., Huang, X., Cheng, J., Zhu, D., and Zhang, X. (2019). High-quality, high-throughput cryo-electron microscopy data collection via beam tilt and astigmatism-free beam-image shift. J. Struct. Biol. *208*, 107396. https://doi.org/10.1016/j.jsb.2019.09.013.

58. Tegunov, D., Xue, L., Dienemann, C., Cramer, P., and Mahamid, J. (2021). Multi-particle cryo-EM refinement with M visualizes ribosome-antibiotic complex at 3.5 Å in cells. Nat. Methods *18*, 186–193. https://doi.org/10.1038/s41592-020-01054-7.

59. Virtanen, P., Gommers, R., Oliphant, T.E., Haberland, M., Reddy, T., Cournapeau, D., Burovski, E., Peterson, P., Weckesser, W., Bright, J., et al. (2020). SciPy 1.0: fundamental algorithms for scientific computing in Python. Nat. Methods *17*, 261–272. https://doi.org/10.1038/s41592-019-0686-2.

Please cite this article in press as: Kong et al., Cryo-electron tomography reveals the packaging pattern of RuBisCOs in *Synechococcus* β-carboxysome, Structure (2024), https://doi.org/10.1016/j.str.2024.05.007

STAR★METHODS

KEY RESOURCES TABLE

REAGENT or RESOURCE	SOURCE	IDENTIFIER
Bacterial and virus strains		
Synechococcus elongatus PCC 7942	This paper	GenBank: CP000100.1
Deposited data		
Atomic coordinates of free RuBisCO	This paper	8WPZ
EM maps of free RuBisCO	This paper	EMD-37727
EM maps of encapsulated RuBisCO	This paper	EMD-37728
EM maps of RuBisCO-SSUL	This paper	EMD-37729
EM maps of RuBisCO loosely attached to the shell	This paper	EMD-37730
EM maps of RuBisCO tightly attached to the shell	This paper	EMD-37731
Software and algorithms		
Warp	Tegunov et al. 2019[39]	http://www.warpem.com/warp/; RRID: SCR_018071
Origin	N/A	https://www.originlab.com/Origin; RRID: SCR_014212
Dynamo	Castaño-Díez et al. 2012[43]	http://www.dynamo-em.org; RRID: SCR_017541
Relion3.1	Bharat and Scheres, 2016[49]	http://www2.mrc-lmb.cam.ac.uk/relion; RRID: SCR_016274
IMOD	Kremer et al. 1996[37]	https://bio3d.colorado.edu/imod/; RRID:SCR_003297
EMAN2	Chen et al. 2017[45]	https://blake.bcm.edu/emanwiki/EMAN2/Programs/tomoseg; RRID: SCR_016867
ChimeraX	Meng et al. 2023[50]	https://www.cgl.ucsf.edu/chimerax/; RRID: SCR_015872
PHENIX	Adams et al. 2010[51]	https://www.phenix-online.org; RRID: SCR_014224
COOT	Emsley and Cowtan, 2004[52]	https://www2.mrc-lmb.cam.ac.uk/personal/pemsley/coot/: RRID: SCR_014222

RESOURCE AVAILABILITY

Lead contact

Further information and requests for resources and reagents should be directed to and will be fulfilled by the Lead Contact, Cong-Zhao Zhou (zcz@ustc.edu.cn).

Materials availability

This study did not generate new unique reagents.

Data and code availability

All study data are included in the article and/or supplemental information. The coordinates of free RuBisCO have been deposited to Protein Data Bank (PDB: 8WPZ). The EM maps of free RuBisCO (EMDB: EMD-37727), encapsulated RuBisCO (EMDB: EMD-37728), RuBisCO-SSUL (EMDB: EMD-37729), RuBisCO loosely attached to the shell (EMDB: EMD-37730), RuBisCO tightly attached to the shell (EMDB: EMD-37731) have been deposited in the Electron Microscopy Data Bank and are publicly available as of the date of publication.

This paper does not report original code.

Any additional information required to reanalyze the data reported in this paper is available from the lead contact upon request.

EXPERIMENTAL MODEL AND STUDY PARTICIPANT DETAILS

For details about the bacterial strains and culture conditions, please refer to the Method details.

Please cite this article in press as: Kong et al., Cryo-electron tomography reveals the packaging pattern of RuBisCOs in *Synechococcus* β-carboxysome, Structure (2024), https://doi.org/10.1016/j.str.2024.05.007

METHOD DETAILS

Growth of cyanobacteria

The *Synechococcus elongatus* PCC 7942 cells were cultured in BG11 medium under atmospheric conditions. The cultures were grown at 30°C in one-liter conical bottles with a rotation speed of 120 rpm and a light intensity of 1000 lux. The chlorophyll content of the cells was determined using the method as described previously.[53]

Purification of β-carboxysomes

Purification of β-carboxysome was performed using the method as described previously.[36] The cells were pelleted by centrifugation at 3500 g for 10 min at 20°C and resuspended in 50 to 100 mL of lysis buffer containing 0.6 M sucrose and 20 mM Tes-NaOH, pH 7.5 to remove excess BG11. The cells were repelleted and then resuspended to 20 mL of lysis buffer containing the egg lysozyme (2 mg/mL) and treated for 2 hr at 35°C in darkness and with slow shaking. The treated cells were recentrifuged at 3500 g, washed in lysozyme buffer, and repelleted. The cells were then resuspended with the buffer of 20 mM Tes-NaOH, pH 7.0, 5 mM EDTA, 50 μg/ml DNAse and protease inhibitor cocktail at a Chl concentration of 0.5 mg/mL. The cells were lyzed by ultrasonication at 25% power for 4 min. The crude extract was centrifuged at 12,000 g (4°C; R20A2 rotor) for 15 min to remove the cell debris. Then 3 volumes of 1×EM buffer (40 mM Epps-NaOH, pH 8.0, and 27 mM $MgSO_4$) containing 20% (v/v) Percoll (Cytiva) and 0.133% Triton X-100 detergent was added to the cell extract containing carboxysome. Then the mixture was incubated on ice for 10 min. Following the precipitation of carboxysomes by the Percoll beads in the presence of Mg^{2+}, the carboxysomes were pooled by centrifugation at 12,000 g (4°C; R20A2 rotor) for 15 min. Afterwards, the pellet was resuspended in 5 mL of 0.75×EM buffer containing 1% Triton X-100 and then repelleted by centrifugation at 12,000 g for 10 min. The pellet was then washed twice in 1 to 2 mL of 0.75×EM buffer followed by centrifugation at 12,000 g for 5 min. Finally, the pellet containing carboxysomes was resuspended in 0.5 mL of 0.75×EM buffer.

SDS-PAGE analysis

The purified β-carboxysome samples were mixed with 5 ×SDS loading buffer. In each well of a 4-20% gradient SDS-PAGE, 10 μL mixture was loaded for gel electrophoresis at 180 V for ~1 hr. Each specific protein band was extracted from the gel and treated with trypsin digestion, and analyzed by liquid chromatography/mass spectrometry (LC-MS/MS) (Thermofisher Q Exactive Plus). The protein components were identified by matching the theoretical fragmentation patterns.

Liquid chromatography mass spectrometry analysis

Proteins were digested using the filter-aided sample preparation (FASP) method.[54] Briefly, the proteins were digested with sequencing grade trypsin with the ratio of 1:50 (w:w) at 37°C overnight. The resultant tryptic peptides were desalted by StageTips.[55] Peptides were analyzed by LTQ Orbitrap Elite mass spectrometer (ThermoFisher Scientific) coupled online to an Easy-nLC 1000 (Thermo Fisher Scientific) in the data-dependent mode. The data was analyzed using the software MaxQuant. The sequence database of β-carboxysome was applied to searching the data. The maximum number of missed cleavages was set at two, iBAQ was selected for protein quantification. The false discovery rate was set at 0.01 for peptide and protein identifications.

Cryo-ET sample preparation and data collection

Vitrobot Mark IV (Thermo Fisher Scientific) was used to prepare the frozen samples. The purified samples were mixed with 6 nm gold particles prior to freezing. A Quantifoil R3.5/1 Cu 200 mesh grid was glow-discharged for 10 sec. Then 3.5 μL of the samples were added to the grid and the excess liquid was blotted by the filter paper for 5 sec with a force of -7 at 8°C and a humidity of 100%. Then, the grid was plunge-frozen in liquid ethane.

Tilt series acquisition

The grids were inserted into the grid cassette of an autoloader and loaded into a Titan Krios transmission electron microscope (Thermo Fisher Scientific) which was equipped with a zero-loss energy filter with a slit width of 20 eV and a K2 Summit direct electron detector (Gatan). Serial EM software[56] was used to acquire the images. Tilt series were acquired at 105 kx magnification (pixel size 1.36 Å) with a dose-symmetric tilt scheme using the beam-shift method.[57] The total dose was set to ~ 145 $e^-/Å^2$ and the tilt range was set at nominal values of -60° to +60° with an increment of 3°. The defocus range was set between -1 and -3 μm. The statistics for tilt series collection are listed in Table S2.

Image processing

Raw images of tilt series were sent into Warp[39] for the motion correction and CTF estimation. Various types of low-quality images were manually removed from the final tilt series dataset. These include samples obstructed by the stage, grid bar, or contaminants; images exhibiting large motions and inaccurate CTF estimations; images containing apparent crystalline ice; or images displaying an apparent discontinuity in the tilt series. After filtering out the low-quality images, 88 tilt series were generated and auto-aligned using Dynamo. Then the alignment parameters were sent back into Warp. The defocus value was set at -2 μm. During subsequent data processing, the computer-fitted defocus value ranged from approximately -1.7 μm to -2.3 μm. The tomograms were reconstructed at a binning level of eight and deconvolved for better visualization. To avoid potential model bias, we did not employ any previously

Please cite this article in press as: Kong et al., Cryo-electron tomography reveals the packaging pattern of RuBisCOs in *Synechococcus* β-carboxysome, Structure (2024), https://doi.org/10.1016/j.str.2024.05.007

reported or published structures in data processing, and only our data-driven maps were used as the reference template in all the classification and refinement jobs.

First, a total of 29 k dispersed RuBisCO particles were manually picked in Dynamo. The sub-tomogram particles in box size of 36^3 voxels were extracted from 8× binned tomograms in Warp. The initial map was directly reconstructed from the input particle star file using the *relion_reconstruct* command in Relion software with the following parameters: *relion_reconstruct –i input.star –o output.mrc –3d_rot –ctf*. The resulting map that incorporated the 3D rotational information and the CTF parameters was used as the initial reference for global 3D classification using C4 symmetry. The better 3D classes of higher resolution and similar structural features to RuBisCO containing 19 k particles were selected for further analysis. Then, the sub-tomogram particles in box size of 48^3 voxels were extracted from 4× binned tomograms in Warp. A 3D classification using local alignment in D4 symmetry was performed and 5.6 k particles were selected. After re-extracting from 2× binned tomograms with a box size of 80^3 voxels, a local refinement was performed to report the resolution to be 5.6 Å. Then 1× binned sub-tomogram particles with a box size of 160^3 voxels were extracted. 2.7 k good particles were selected after local 3D classification, and its resolution was estimated to be 3.9 Å by applying D4 symmetry based on the ''gold-standard'' Fourier Shell Correlation (FSC) with 0.143 criterion after auto-refinement in Relion[49] and M.[58] The RuBisCO model was built by fitting the structure of *Synechococcus elongatus* PCC 6301 RuBisCO (PDB: 1RSC) into the 3.9 Å map using ChimeraX.[50] Then the structure was manually rebuilt in COOT[52] and automatically refined by real space refinement in PHENIX.[51] The statistics of data processing, model building and refinement of free RuBisCO were listed in Table S3.

Second, a total of 83 k RuBisCO particles were picked using template matching method in Dynamo. The sub-tomogram particles in box size of 48^3 voxels were extracted from 4× binned tomograms in Warp. The direct reconstruction map was used as the initial single reference for local 3D classification using C1 symmetry, then the better classes containing 41 k particles were chosen. In another round of 3D classification using D2 symmetry, using the best map (free RuBisCO) from a previous job as the single reference, 21 k RuBisCO particles and 8.7 k RuBisCO-SSUL particles were classified and selected respectively. After re-extracting from 2× binned tomograms with a box size of 80^3 voxels, 7.6 k RuBisCO particles in D4 symmetry and 3.6 k RuBisCO-SSUL particles in D2 symmetry were selected respectively using local 3D classification. Then 1× binned sub-tomogram particles with a box size of 160^3 voxels were extracted. The resolutions of RuBisCO and RuBisCO-SSUL maps were estimated to be 4.4 Å (D4 symmetry) and 5.9 Å (D2 symmetry) respectively after auto-refinement in Relion and M. The local cross-correlations between SSUL module and the maps were calculated by the real space refinement implemented in PHENIX.[51] The maps and coordinate files were uploaded in the program *phenix.real_space_refine*, yielding the output cross-correlation (CC) values.

Finally, the shell of carboxysomes were traced using surface model in Dynamo, and the coordinates and orientations of 53 k shell-attached RuBisCO particles were generated using oversampling method. The sub-tomogram particles in box size of 64^3 voxels were extracted from 8× binned tomograms in Warp. The direct reconstructed map was used as the initial reference for 3D classification using C2 symmetry, then the better classes containing 18 k particles were chosen. Then, the sub-tomogram particles in box size of 64^3 voxels were extracted from 4× binned tomograms in Warp for 3D classifications. After several rounds of local 3D classifications in C4 symmetry from 2× binned tomograms with a box size of 96^3 voxels, two best classes possessing 2.3 k and 3.5 k particles yield the cryo-EM maps of 8.4 and 8 Å, respectively.

Calculation of the volume and RuBisCO density of β-carboxysome

The Delaunay method[59] was used to calculate the volume of a carboxysome. First, we selected hundreds of points at the shell and assigned the precise coordinates in the tomogram of each carboxysome. Then we randomly divided the set of three-dimensional points into numerous triangles, which could further separate the carboxysome into triangular cones formed by these triangles and the reference points inside the carboxysome. The volume of a carboxysome was calculated by employing the sum of the volumes of these triangular cones. The RuBisCO density in β-carboxysome is calculated by dividing the volume of a carboxysome by the total number of RuBisCO.

Statistical analysis of RuBisCO arrangements in β-carboxysome

The statistical analysis of RuBisCO arrangement was performed in a similar method as reported previously.[30] The refined subtomograms were mapped back to the tomograms according to their positions and orientations. Then relative orientations of their 4-fold axes of each RuBisCO pair in a carboxysome were calculated. For each RuBisCO pair (A and B), the constraint parameters are as follows: (i) The distance from the center point of RuBisCO A to the center plane of the orthogonal axis line of RuBisCO_B. (ii) The distance from the center point of RuBisCO_B to the center plane of the orthogonal axis line of RuBisCO_A. (iii) The angle between the 4-fold axis lines of RuBisCO_A and RuBisCO_B. Each pair of adjacent RuBisCO in carboxysome is divided into the following three categories based on the following criteria: (1) head-to-head: distance>68 nm, angle<35 degrees; (2) head-to-side: distance>68 nm and distance<28 nm, angle>65 degrees; (3) side-to-side: distance<28 nm, angle<35 degrees.

The ideal modeling of RuBisCO arrangements in β-carboxysome

In terms of morphological analysis, we compared the distinctive projections of an icosahedron along its three symmetric axis and the corresponding projections of actual carboxysomes (Figure 6B). These projections exhibit three primary shapes: a regular hexagon, a symmetrical hexagon formed by combining two isosceles trapezoids, and a regular decagon.

First, we conducted statistical analysis using the regularly shaped hexagonal slice images. Assuming an edge length of *l* nm for the skeleton of an icosahedron, in the case of a regular hexagonal slice, the actual interpretation is a cross-sectional image that is parallel

Please cite this article in press as: Kong et al., Cryo-electron tomography reveals the packaging pattern of RuBisCOs in *Synechococcus* β-carboxysome, Structure (2024), https://doi.org/10.1016/j.str.2024.05.007

to the triangular faces at the top and passes through the center of the carboxysome. The actual shape of this cross-section is a dodecagon, which comprises two internal angles measuring 135.521° and 164.479°, respectively. However, due to the limited resolution, the angle of 164.479° is approximated as 180°. Consequently, the dodecagon is recognized as a regular hexagon, with a side length of ~0.875*l*.

In the tomogram, the side length of the shell is closely associated with the number of RuBisCO, with a minimal distance about 0.2× 2*r* nm between adjacent RuBisCOs (*r* is the radius of RuBisCO). Consequently, the outermost layer of the icosahedron contains $n = \left\lfloor \frac{l}{(2+0.2\times2)r} + 0.5 \right\rfloor$ RuBisCO along each edge. Moreover, on each layer of the icosahedron, there are $10n^2$-20n+12 RuBisCOs. We manually counted the number of RuBisCO in the outermost layer of the carboxysome and compared them to the theoretical number of RuBisCO calculated by the formula.

We selected 45 carboxysomes with relatively regular shapes and analyzed each side corresponding to the triangular region of hexagonal structures. Notably, the number of internal layers corresponds to the number of RuBisCO present in the outermost layer, with a gradual decrease in the number of RuBisCO from the outermost to the innermost layer. RuBisCOs in the inner layers were generally arranged in the same way as the outermost layer.

QUANTIFICATION AND STATISTICAL ANALYSIS

Softwares required for quantification and statistical analyses include Warp, Origin, Dynamo, Relion3.1, IMOD, EMAN2, ChimeraX, PHENIX and COOT. Cryo-ET data collection statistics were summarized in Table S2. The statistics of data processing, model building and refinement for the free RuBisCO structure are listed in Table S3.